THE JOURNAL OF PHYSICAL CHEMISTRY C
A JOURNAL OF THE AMERICAN CHEMICAL SOCIETY

pubs.acs.org/JPCC
Article

Oxidative Ring-Opening of Dimethylfuran in Zeolitic Imidazolate Frameworks through Computational Design

Thanh-Hiep Thi Le, Mohammad Reza Alizadeh Kiapi, Dhruv Menon, David Fairen-Jimenez, and Manuel A. Ortuño*

Cite This: *J. Phys. Chem. C* 2026, 130, 3245−3252
Read Online

ACCESS | Metrics & More | Article Recommendations | Supporting Information

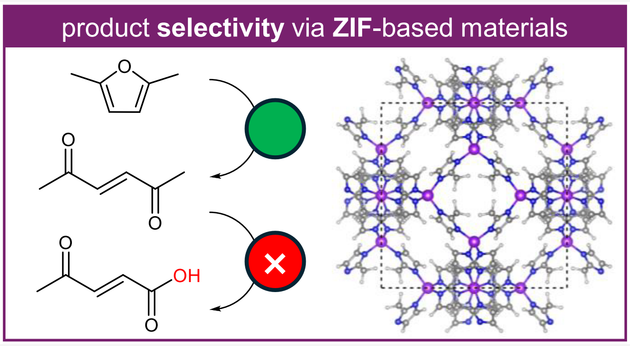

ABSTRACT: Furans are versatile feedstocks for producing valuable chemicals and fuels, with 2,5-dimethylfuran (DMF) particularly standing out for its potential in oxidative ring-opening reactions, yielding enediones. The zeolitic imidazolate framework ZIF-8 has shown promise as a mediator to achieve high selectivity, although a precise mechanistic understanding of how this heterogeneous system works is unclear. Here, we employ a computational protocol, combining a configurational search with force fields (GFN-FF) with a refinement at the periodic density functional theory (DFT) level, to model the oxidation of DMF with H_2O_2 and explicit MeOH solvent in the absence and presence of ZIF-8. In line with experimental observations, our results reveal that ZIF-8 suppresses overoxidation of the enedione *cf.* to results for the blank reaction. We further substituted the methyl group of ZIF-8 with other groups and tested the resulting materials in the above-mentioned reaction. We observe that vinyl-substituted ZIF emerges as the most selective material, while ZIF-H (SALEM-2) offers poor selectivity when compared with the blank reaction. A featurization study, correlating energy barriers and structural features, reveals how pore accessibility and linker geometry influence the selectivity. Our findings seek to deepen the understanding of molecular interactions in ZIFs and guide the rational design of MOFs for biomass conversion.

■ INTRODUCTION

Biomass-derived furans are gaining significant attention as renewable feedstocks for the production of high-value chemicals and fuels.[1−4] Their furan ring exhibits dual reactivity due to its relatively low aromaticity, enabling transformations characteristic of both aromatic compounds and alkenes.[5] The oxidation of furans is among the most prominent methods for producing valuable aliphatic and alicyclic compounds; however, challenges persist in achieving high selectivity by minimizing undesirable byproducts, as well as in developing cost-effective and environmentally friendly oxidants and catalysts.[6−8]

The feedstock 2,5-dimethylfuran (DMF) can be easily obtained from biomass carbohydrates,[9] and its oxidative ring-opening reaction provides direct access to enediones. The majority of early[10,11] and recent[12,13] reports focus on homogeneous systems, which may present limitations at industrial scales. Heterogeneous catalysts, on the other hand, are more suitable for industrial applications due to their robustness and recyclability, but research on them is scarce. Wahlen et al. reported the oxidation of DMF with the zeolite titanium silicate 1 (TS-1) and H_2O_2 in acetonitrile, obtaining 3-hexene-2,5-dione with 85% selectivity.[14] Later, Miedziak et al. employed Au and Au/Pd nanoparticles and O_2 in solvent-free conditions to convert DMF into 3-hexene-2,5-dione, obtaining up to 80% selectivity.[15] We thus envisage room for improvement in the field of heterogeneous materials.

Inspired by the success of zeolites,[14] we turned to metal−organic frameworks (MOFs),[16] a family of porous materials formed by inorganic nodes connected via organic linkers. MOFs have already shown promise in biomass upgrading applications.[17,18] In 2021, Franco et al. reported the oxidation of DMF with H_2O_2 in methanol to form 3-hexene-2,5-dione in the presence of the zeolitic imidazolate framework ZIF-8 with up to 85% selectivity.[19] At a similar high DMF conversion, the blank run yielded only 27% selectivity, with 4-oxo-2-pentenoic acid as the main side product coming from a Baeyer−Villiger oxidation (Figure 1). Interestingly, performing the reaction with the unassembled ZIF-8 components (i.e., Zn^{2+} ions and 2-methylimidazolate ligands) provided only 30% selectivity, which highlights the key role of the porous network. To the

Received: September 23, 2025
Revised: February 11, 2026
Accepted: February 13, 2026
Published: February 19, 2026

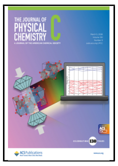

ACS Publications

https://doi.org/10.1021/acs.jpcc.5c06617

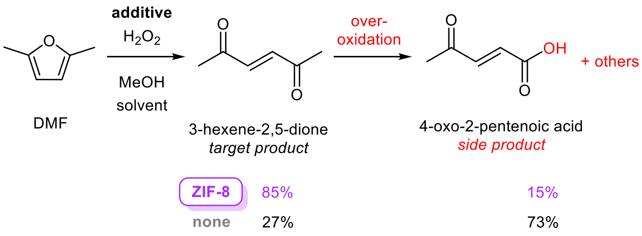

Figure 1. Oxidative ring-opening of DMF with H_2O_2 in the presence and absence of ZIF-8, including product selectivity.

best of our knowledge, this is the only MOF-based contribution to date.

These encouraging results motivated us to investigate the mechanistic details of the process involving ZIFs.[20] These systems are amenable to linker modification,[21] enabling precise control over pore size, framework topology, and surface chemistry, thus tuning the stability, hydrophobicity, and hydrophilicity of the materials.[22,23] Here, we study the role of ZIF-8 in selectivity control using computational techniques.[24] We model the oxidative ring-opening of DMF with H_2O_2 with explicit methanol solvent, with and without ZIF-8, as reported experimentally.[19] We follow a multilevel approach where we first perform an exhaustive conformational search at a low level of theory (force field) and then refine the energies and structures at the quantum mechanical level (periodic density functional theory). We compute the thermodynamic profile of the reaction, considering only the key transition states that control selectivity. Finally, we investigate structural features that potentially predict the performance of other ZIFs, with the aim of guiding further experimental design.

■ COMPUTATIONAL SECTION

Models

For isolated molecules, we used a cubic unit cell with a cell length of 20 Å. For ZIF-8, we employed two different approaches. We first considered a cubic unit cell with a cell length of 17.056 Å and 276 atoms, as reported in the literature (Figure 2a).[25] From the periodic structure, we then prepared a finite-size cluster with 480 atoms to represent the full cavity, which was defined by six 4-ring and eight 6-ring windows (Figure 2b). Nodes were capped with OH^- and H_2O to maintain the Zn coordination environment and charge neutrality. These groups were pointing outward of the cavity and did not interact with the host species.

Methods

Our computational protocol entails a (**i**) fast but extensive conformational search with a force field using a finite-size cluster model; from there, we selected several low-energy structures and performed a (**ii**) refinement of energies and geometries at the density functional theory (DFT) level with periodic models. This strategy allows us to efficiently explore the potential energy surface and ensure that the most relevant conformers are considered. For the sake of clarity, only the most stable species are reported and discussed at the DFT level in the text. We used this protocol for both blank and MOF-mediated reactions.

Regarding the initial step (**i**), the finite-size cluster models were computed with the GFN-FF force field[26] as implemented in the *xtb* 6.4.1 software package.[27] We performed an automatic conformational search with CREST[28] for each reaction intermediate and transition state (TS) within the ZIF pores. During that search, the host framework was fixed[29] and the guest molecules were free. In the case of TS guest molecules, selected bond distances were constrained to preserve the structure. As for the refinement step (**ii**), the periodic models were computed in the gas phase with the PBE density functional[30] as implemented in VASP.[31,32] The Grimme D3 scheme[33] with the Becke−Johnson damping function[34] was employed to account for dispersion interactions. Core electrons were represented using projector augmented wave (PAW) pseudopotentials,[35] and valence electrons were expanded in a plane-wave basis set with a kinetic energy cutoff of 600 eV for cell optimization. After that, the cell parameters were kept fixed and all subsequent calculations are reported with a kinetic cutoff of 450 eV. The Brillouin zone was sampled at the Γ-point, employing the Monkhorst−Pack method.[36] TS structures were obtained using the climbing image nudged elastic band (CI-NEB)[37] and improved dimer[38] algorithms. Minima and TSs were characterized by diagonalizing the numerical Hessian matrix, allowing displacements of ±0.015 Å. Electronic energies were converged to 10^{-6} eV, and geometries were optimized until the forces on the atoms were less than 0.025 eV/Å. During geometry optimizations, the positions of all atoms in the system were allowed to relax without restrictions. Vibrational partition functions were computed using numerical frequen-

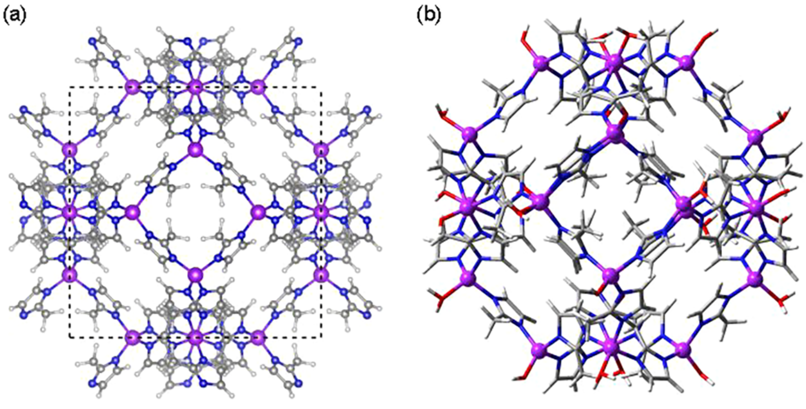

Figure 2. (a) Periodic structure (unit cell in dashed black lines) and (b) finite-size cluster of ZIF-8. Atom legend: Zn (purple), O (red), N (blue), C (gray), H (white).

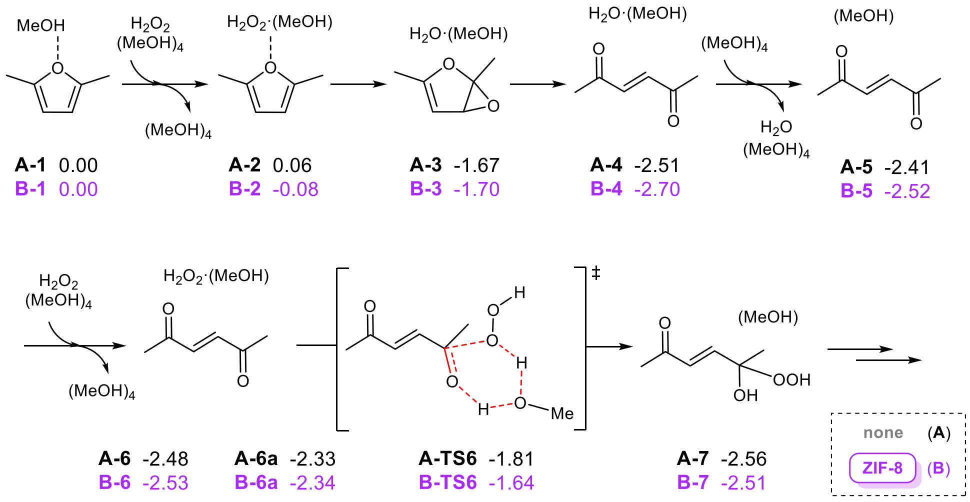

Figure 3. Intermediates in the ring-opening oxidation of DMF to 3-hexen-2,5-dione with H_2O_2 in the absence (black) and presence (purple) of ZIF-8. Gibbs energies at the PBE-D3(BJ) level in eV.

cies, where only selected atoms were allowed to move. Frequencies below 100 cm^{-1} were shifted to 100 cm^{-1} when computing vibrational partition functions. All thermochemical properties were calculated using tools4VASP[39] at 333 K, as reported experimentally.[19]

Finally, we carried out a small benchmark study of selected species for the reaction in the absence of ZIF-8. Gaussian 16[40] was employed to perform single-point calculations with the def2-TZVP basis set[41] using several density functionals with D3(BJ) corrections (except for Minnesota functionals): PBE,[30] BLYP,[42,43] TPSS,[44] M06-L,[45] PBE0,[46] B3LYP,[47] TPSSh,[44,48] and M06.[49] ORCA 5.0[50] was also employed to perform single-point calculations with the def2-TZVP basis set[41,51] using the DLPNO−CCSD(T)[52] level of theory.

All energies and geometries reported herein are freely available in the open-access[53] ioChem-BD platform[54] through the following database.[55]

Featurization

Atomic positions and cell parameters of ZIF candidates were optimized using periodic DFT (see above), after which their structural features were converted into fixed-sized arrays using the MOFDSCRIBE package.[56−58] It is noted that the current model does not account for linker swing motion found in ZIF-8.[59] Several descriptors were selected, including building unit features (inertial shape factor,[60,61] shape of linkers,[62] pairwise distances[56,63]), and pore geometry features such as accessible volume, pore diameters, and accessible surface area.[64,65] In that respect, a radii probe of 1.7 Å (half of the diameter pore aperture in ZIF-8) was chosen. The Pearson correlation coefficient *r* was then calculated using appropriate features (see the Supporting Information for details). To visualize the correlation matrix, a Seaborn heatmap was used as implemented in the Seaborn package.[66]

■ RESULTS AND DISCUSSION

To elucidate the role of ZIF-8 as a mediator in promoting selectivity, we first computed the blank oxidation process using H_2O_2 in explicit MeOH solvent and compared it with that including the periodic structure of ZIF-8. We then explored the adsorption of related furan-based feedstocks. Finally, we tuned the linkers of ZIF-8 to predict the selectivity trends when using related materials as mediators. We reiterate that only the most stable structures are reported here, which were obtained after performing a configurational search at a low level (finite-size model with GFN-FF) followed by geometry and energy refinement at a high level (periodic model with PBE-D3(BJ)).

Blank Reaction

Figure 3 shows the main intermediates in the ring-opening oxidation of DMF to 3-hexen-2,5-dione with H_2O_2 in the absence of ZIF-8 (**A**). To properly describe the solvation environment, we include the solvent explicitly. After testing several models (Figure S1), we compute the reacting substrates with one methanol molecule and nonparticipating molecules with four methanol molecules. Initially, solvated DMF **A-1** (0.00 eV, energy reference) first forms an isoenergetic adduct with H_2O_2 **A-2** (0.06 eV). Oxidation of one double bond yields an epoxide and H_2O **A-3** (−1.67 eV), which can further evolve via ring-opening to give 3-hexen-2,5-dione **A-4** (−2.51 eV). In the presence of excess oxidant, the reaction might continue. Removal of H_2O in **A-5** (−2.41 eV) and addition of a second equivalent of H_2O_2 in **A-6** (−2.48 eV) prepare the system for Baeyer−Villiger oxidation of the ketone group. We did not study the entire reaction, which is reported elsewhere.[67,68] Since we are interested in selectivity, we only focused on the nucleophilic attack TS to estimate the energy required to start the pathway toward side products. Thus, from **A-6** (−2.48 eV) and after a conformational reorganization of the substrates in **A-6a** (−2.33 eV),[69] the transition state **A-TS6** (−1.81 eV) describes the nucleophilic attack of H_2O_2 on the ketone group with concomitant proton transfer to yield a Criegee intermediate **A-7** (−2.56 eV). This process has a Gibbs energy barrier of 0.70 eV. Subsequent steps not computed herein would eventually yield 4-oxo-2-pentenoic acid.

For the blank reaction, we computed the energy barriers with several density functionals and found that GGA functionals yield lower values than hybrid ones, with those being closer to those of DLPNO−CCSD(T) (Table S1). Since we are interested in comparing the blank reaction against the ZIF-mediated reaction, systematic errors would follow the same trend. In other words, energy barriers at PBE-D3(BJ) may be underestimated, but the reactivity trend between systems should hold.

ZIF-8-Mediated Reaction

After studying the blank reaction, we computed the pathway inside the pore of ZIF-8 (**B**) including the solvent explicitly. The main intermediates also shown in Figure 3 are mostly the same, except for some minor conformational changes due to the different environment. From **B-1** (0.00 eV, energy reference), the adduct **B-2** (−0.08 eV) is still isoenergetic, and the subsequent epoxide **B-3** (−1.70 eV) and dione **B-4** (−2.70 eV) follow the previous trend. Regarding the overoxidation, the thermodynamics of **B-5** (−2.52 eV), **B-6** (−2.53 eV), **B-6a** (−2.34 eV),[69] and **B-7** (−2.51 eV) is quite similar to the blank reaction. But interestingly, the nucleophilic attack via **B-TS6** (−1.64 eV) is more energetically demanding.

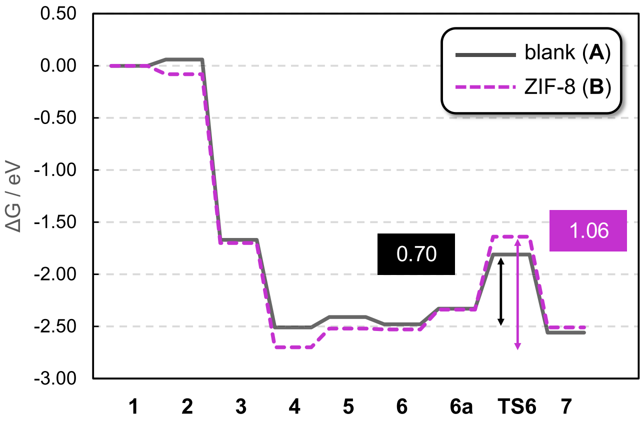

Figure 4. Gibbs energy profiles of the ring-opening oxidation of DMF without (black line) and with ZIF-8 (purple line). Intermediates are shown in Figure 3. Gibbs energies at the PBE-D3(BJ) level in eV.

For a better comparison, Figure 4 shows the Gibbs energy profiles of the blank reaction (solid black line) and the ZIF-8-mediated reaction (dashed purple line). One can see the similarity of both profiles except for two key structures: the target product 3-hexen-2,5-dione **4** and the transition state leading to overoxidation **TS6**. Inside ZIF-8, the former is lower by 0.19 eV (*cf.* blank) and the latter is higher by 0.17 eV (*cf.* blank). As a result, the net Gibbs energy barriers of overoxidation for blank and ZIF-8-mediated reactions are 0.70 and 1.06 eV, respectively; that is, the formation of side products is disfavored by 0.36 eV when the framework is present.

To further explore the origin of these differences, Figure 5 shows the optimized structures of key species **4** and **TS6** (additional structures can be consulted in Figure S2). On the one hand, intermediate **4** is slightly more stable inside ZIF-8 than in its absence by 0.19 eV. We attribute this trend to the presence of noncovalent interactions.[70] Due to the hydrophobicity of the pore,[71] these dispersion-driven interactions can also be extrapolated to other intermediates. On the other hand, transition state **TS6** is slightly more disfavored inside ZIF-8 than in its absence by 0.17 eV. This could be related to the need of space to adopt a rather organized transition state.[72] Having said that, it is worth noting that the individual differences are not particularly large (less than 0.2 eV); thus, it is not straightforward to pinpoint the precise interactions that create such a trend. Nevertheless, we believe that this is not related to configurational noise, as we have previously explored the chemical space in a thorough way.

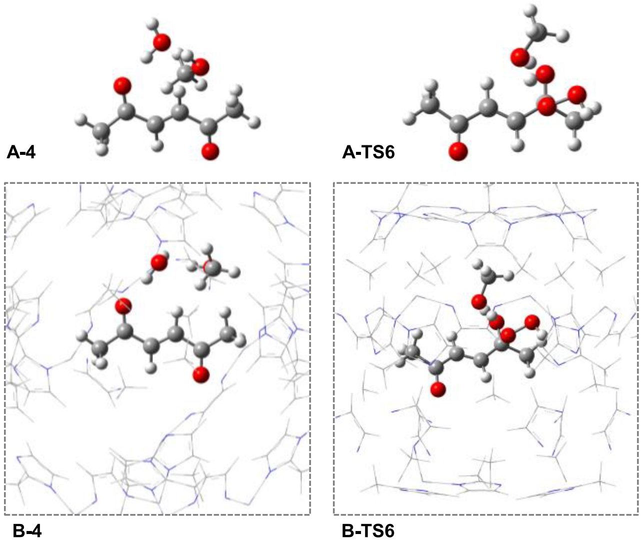

Figure 5. PBE-D3(BJ)-optimized structures of intermediate 4 and **TS6** in the absence (**A**) and presence (**B**) of ZIF-8.

Behavior of Other Furans

Although experimental work has mainly focused on the oxidation of DMF, the reactivity of other furans such as furfural (FUR), furfuryl alcohol (FAL), and 5-(hydroxymethyl)furfural (HMF) was also tested, but with no success.[19] Thus, we wondered whether our current model could provide a qualitative explanation for this observation. While computing the full thermodynamics for all variants is out of the scope of the present work, we did, however, consider their initial adsorption inside the ZIF-8 pores. Following the previous protocol and model, we computed the reaction energy associated with the adsorption of furans solvated by 4 MeOH molecules, as shown in Figure 6. The resulting Gibbs energy differences were −0.14, 0.08, 0.32, and 0.39 eV for DMF, FUR, FAL, and HMF, respectively. It is worth noting that only the step involving DMF is exoergic, while the other compounds are isoenergetic or endoergic. Despite the simplicity of these calculations, they already provide a reasonable trend for furans, showing that more hydrophilic species are less likely to interact with the framework, as suggested experimentally.

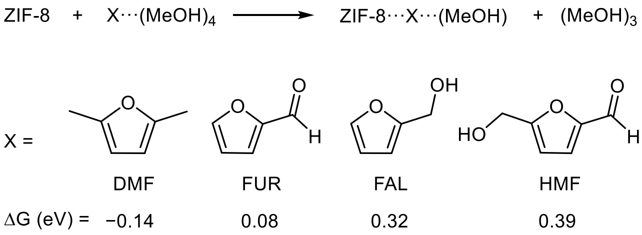

Figure 6. Reaction Gibbs energies for the adsorption of solvated furans inside ZIF-8. Gibbs energies at the PBE-D3(BJ) level in eV.

Prediction of Selectivity Enhancement

Building on the previous results that can qualitatively simulate the experimental trends, we now investigate whether other ZIFs can enhance the selectivity of the reaction. Previous studies have pointed out the impact of linker exchange on the interaction between host material and guest molecule.[73] Thus, we prepared six ZIF-based structures (with the same sodalite topology) using 2-substituted imidazolate linkers, where $-CH_3$ was exchanged by different organic groups. We employed $-C{\equiv}CH$,[74] $-CH{=}CH_2$,[75] −Br,[76,77] −Cl,[76,77] −H,[78] and −CHO,[79] referring to them as ZIF-Ethynyl, ZIF-Vinyl, ZIF-Br, ZIF-Cl, ZIF-H (also SALEM-2), and ZIF-CHO (also ZIF-90), respectively (Figure 7a). For computational efficiency, we used the ZIF-8 unit cell for the six modified ZIFs as the linker substitutions were relatively minor.[80] With the new candidates in hand, we computed the adsorption energies following the scheme in Figure 6. All processes were exoergic with values of −0.29, −0.21, −0.36, −0.19, −0.16, and −0.30 eV, respectively. We then computed the simplified Gibbs energy profiles (Figure S3) and the Gibbs energy barriers for the overoxidation (Figure 7b). Taken as reference the blank value of 0.70 eV, all materials perform better except for ZIF-H with 0.75 eV, from which low selectivity would be expected. Taken as reference the ZIF-8 value of 1.06 eV, most materials perform slightly worse except for ZIF-CHO with 1.11 eV and ZIF-Vinyl with 1.27 eV, for which similar and enhanced selectivities would be expected. These barriers seem to be influenced by more than just the electron-donating or -withdrawing nature of the substituents, pointing to other properties that might also play a role. Thus, we next study the impact of linker modifications on both the topology of linkers and the pore structure in further detail.

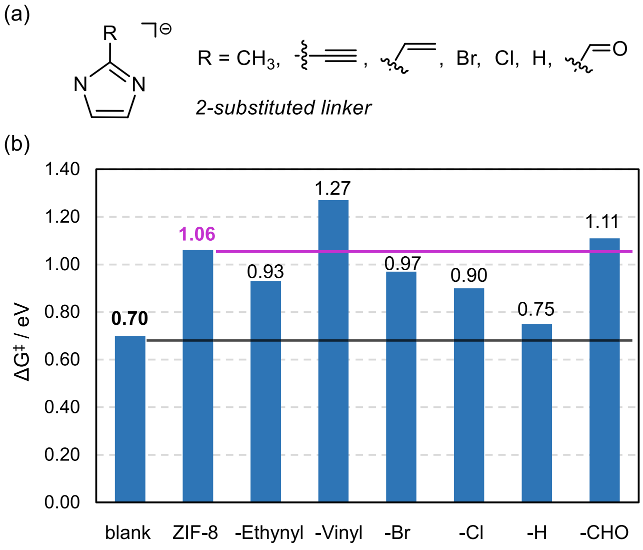

Figure 7. (a) Linker modifications of ZIF materials and (b) Gibbs energy barriers of overoxidation for the blank and all of the materials. Gibbs energies at PBE-D3(BJ) level in eV.

Correlating Energy Barriers and Structural Properties

In an attempt to rationalize structure−property relationships that affect the energy barriers, we performed a featurization study of the designed MOFs to extract the main descriptors using MOFDSCRIBE.[56] Different features were selected to describe the pore properties, including probe accessible volume, pore diameters, and probe accessible surface areas, along with the chemistry of the building unit, including inertial shape factor and shape of linkers (only linkers were displayed due to unchanged Zn node). Previous computed adsorption energies are also included. A detailed explanation of all descriptors can be found elsewhere.[57,58]

All data are collected as a heatmap in Figure 8. We first note that there is a negligible correlation between the energy barriers and the adsorption energies. We then observed that, when using a 1.7 Å probe, accessible volume values of the ZIFs are divided into two groups: one that allows access (ZIF-8, ZIF-Vinyl, and ZIF-CHO), and another one that does not (ZIF-Ethynyl, ZIF-Br, ZIF-Cl, and ZIF-H). The accessible group exhibits a strong positive correlation with energy barriers, and the same trend is also observed for the accessible surface area. For pore diameters, we calculated the largest

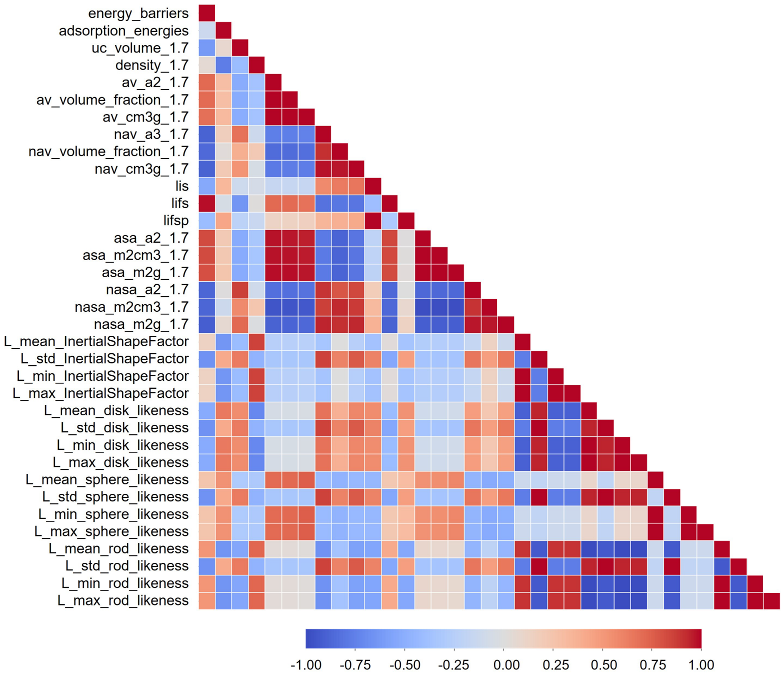

Figure 8. Correlation diagram from the featurization of seven ZIF-based materials, including Gibbs energy barriers. L = linker.

included sphere (lis), largest free sphere (lifs), and largest included sphere along free sphere path (lifsp).[81] ZIF-Vinyl has the highest lifs value (3.67 Å), followed by ZIF-CHO (3.49 Å) and ZIF-8 (3.43 Å), and the least lifs value is found in ZIF-H (3.18 Å), resulting in differences in how freely guest molecules can access the pores. Then, we explored the correlation between linker shape features; specifically, rod- and sphere-like features are positively correlated with energy barriers, whereas disk-likeness shows a negative correlation. Additionally, we computed a histogram and statistical analysis of pairwise distances (Figure S4). The mean pairwise interatomic distances are 8.29 Å for ZIF-Vinyl, 8.24 Å for ZIF-CHO, 8.20 Å for ZIF-8, and 8.14 Å for ZIF-Ethynyl, with the smallest value of 8.08 Å found in ZIF-H.

These results highlight how linker substitutions can alter the size, shape, and distribution of pore apertures, which subsequently impact guest molecule diffusion and adsorption. This, in turn, influences the energy barriers, ultimately helping to reduce the formation of side products and improve selectivity control. Nevertheless, we point out that our modest MOF sample size could limit such correlations, and additional data would be required to make more robust predictions.

■ CONCLUSIONS

Our study investigates the ring-opening oxidation of DMF mediated by various ZIF-based materials. Simulations show that, while the oxidation is favorable both in the presence or absence of ZIF-8, the overoxidation is reduced within the framework, in agreement with available experimental data. Among the new materials tested for this reaction, vinyl-substituted ZIF exhibits the best performance, and ZIF-H exhibits the worst one. A subsequent featurization study indicates that the accessible volume and surface area are strongly correlated with energy barriers, where ZIF-H exhibits the highest nonaccessible volume and surface area, in line with the predicted suboptimal performance. We also observe that linkers with a more linear or elongated configuration, resembling between rod-likeness and sphere-likeness, contribute to enhance selectivity. These insights provide valuable knowledge for future experimental testing and the rational design of MOFs for the conversion of furans, paving the way for improved efficiency and selectivity.

■ ASSOCIATED CONTENT

Supporting Information

The Supporting Information is available free of charge at https://pubs.acs.org/doi/10.1021/acs.jpcc.5c06617.

Additional reaction profiles and statistical analysis (PDF)

■ AUTHOR INFORMATION

Corresponding Author

Manuel A. Ortuño − *Centro Singular de Investigación en Química Biolóxica e Materiais Moleculares (CIQUS), Universidade de Santiago de Compostela, 15782 Santiago de Compostela, Spain; Departamento de Química Física, Universidad de Alicante, 03080 Alicante, Spain;* orcid.org/0000-0002-6175-3941; Email: manuel.ortuno@ua.es

Authors

Thanh-Hiep Thi Le − *Centro Singular de Investigación en Química Biolóxica e Materiais Moleculares (CIQUS), Universidade de Santiago de Compostela, 15782 Santiago de Compostela, Spain*

Mohammad Reza Alizadeh Kiapi − *The Adsorption & Advanced Materials Laboratory (A^{2}ML), Department of Chemical Engineering & Biotechnology, University of Cambridge, Cambridge CB3 0AS, U.K.*

Dhruv Menon − *The Adsorption & Advanced Materials Laboratory (A^{2}ML), Department of Chemical Engineering & Biotechnology, University of Cambridge, Cambridge CB3 0AS, U.K.;* orcid.org/0000-0001-6264-8660

David Fairen-Jimenez − *The Adsorption & Advanced Materials Laboratory (A^{2}ML), Department of Chemical Engineering & Biotechnology, University of Cambridge, Cambridge CB3 0AS, U.K.;* orcid.org/0000-0002-5013-1194

Complete contact information is available at: https://pubs.acs.org/10.1021/acs.jpcc.5c06617

Notes

The authors declare no competing financial interest.

■ ACKNOWLEDGMENTS

This work was funded by MICIU/AEI/10.13039/501100011033 and FSE+ (RYC2022-035453-I, PID2020-119116RA-I00), Xunta Distinguished Researcher program (ED431H 2020/21), the Xunta de Galicia (Centro de Investigación do Sistema Universitario de Galicia accreditation 2023-2027, ED431G 2023/03), and the European Union (European Regional Development Fund−ERDF). The authors acknowledge CESGA ("Centro de Supercomputación de Galicia") for providing generous computational resources. M.R.A.K. acknowledges support from the Cambridge Trust Scholarship and the Trinity Henry-Barlow Scholarship. D.M. acknowledges NanoDTC Cambridge−EPSRC EP/S022953/1. D.F.-J. acknowledges funding by U.K. Research and Innovation (UKRI) under the U.K. government's Horizon Europe funding guarantee (10057499).

■ REFERENCES

(1) Román-Leshkov, Y.; Barrett, C. J.; Liu, Z. Y.; Dumesic, J. A. Production of Dimethylfuran for Liquid Fuels from Biomass-Derived Carbohydrates. *Nature* **2007**, *447*, 982−985.

(2) Caes, B. R.; Teixeira, R. E.; Knapp, K. G.; Raines, R. T. Biomass to Furanics: Renewable Routes to Chemicals and Fuels. *ACS Sustainable Chem. Eng.* **2015**, *3*, 2591−2605.

(3) Wu, L.; Moteki, T.; Gokhale, A. A.; Flaherty, D. W.; Toste, F. D. Production of Fuels and Chemicals from Biomass: Condensation Reactions and Beyond. *Chem* **2016**, *1*, 32−58.

(4) Brun, N.; Hesemann, P.; Esposito, D. Expanding the Biomass Derived Chemical Space. *Chem. Sci.* **2017**, *8*, 4724−4738.

(5) Balaban, A. T.; Oniciu, D. C.; Katritzky, A. R. Aromaticity as a Cornerstone of Heterocyclic Chemistry. *Chem. Rev.* **2004**, *104*, 2777−2812.

(6) Teong, S. P.; Li, X.; Zhang, Y. Hydrogen Peroxide as an Oxidant in Biomass-to-Chemical Processes of Industrial Interest. *Green Chem.* **2019**, *21*, 5753−5780.

(7) Luo, X.; Li, Y.; Gupta, N. K.; Sels, B.; Ralph, J.; Shuai, L. Protection Strategies Enable Selective Conversion of Biomass. *Angew. Chem., Int. Ed.* **2020**, *59*, 11704−11716.

(8) Jaswal, A.; Singh, P. P.; Mondal, T. Furfural – a Versatile, Biomass-Derived Platform Chemical for the Production of Renewable Chemicals. *Green Chem.* **2022**, *24*, 510−551.

(9) Saha, B.; Abu-Omar, M. M. Current Technologies, Economics, and Perspectives for 2,5-Dimethylfuran Production from Biomass-Derived Intermediates. *ChemSusChem* **2015**, *8*, 1133−1142.

(10) Adger, B. M.; Barrett, C.; Brennan, J.; McKervey, M. A.; Murray, R. W. Oxidation of Furans with Dimethyldioxirane. *J. Chem. Soc., Chem. Commun.* **1991**, *21*, 1553−1554.

(11) Finlay, J.; McKervey, M. A.; Gunaratne, H. Q. N. Oxidations Catalyzed by Rhenium(V) Oxo Species 1. Conversion of Furans to Enediones Using Methyltrioxorhenium and Urea Hydrogen Peroxide. *Tetrahedron Lett.* **1998**, *39*, 5651−5654.

(12) Asta, C.; Conrad, J.; Mika, S.; Beifuss, U. Laccase-Catalyzed Stereoselective Oxidative Ring Opening of 2,5-Dialkylfurans into 2-Ene-1,4-diones Using Air as an Oxidant. *Green Chem.* **2011**, *13*, 3066−3069.

(13) Yang, L.; Wang, J.; Wang, Y.; Li, X.; Liu, W.; Zhang, Z.; Xie, X. Stereoselective Synthesis of *cis*-2-Ene-1,4-diones via Aerobic Oxidation of Substituted Furans Catalyzed by ABNO/HNO_3. *J. Org. Chem.* **2021**, *86*, 14311−14320.

(14) Wahlen, J.; Moens, B.; De Vos, D. E.; Alsters, P. L.; Jacobs, P. A. Titanium Silicalite 1 (TS-1) Catalyzed Oxidative Transformations of Furan Derivatives with Hydrogen Peroxide. *Adv. Synth. Catal.* **2004**, *346*, 333−338.

(15) Miedziak, P. J.; Edwards, J. K.; Taylor, S. H.; Knight, D. W.; Tarbit, B.; Hutchings, G. J. Gold as a Catalyst for the Ring Opening of 2,5-Dimethylfuran. *Catal. Lett.* **2018**, *148*, 2109−2116.

(16) Furukawa, H.; Cordova, K. E.; O'Keeffe, M.; Yaghi, O. M. The Chemistry and Applications of Metal-Organic Frameworks. *Science* **2013**, *341*, No. 1230444.

(17) Herbst, A.; Janiak, C. MOF Catalysts in Biomass Upgrading Towards Value-Added Fine Chemicals. *CrystEngComm* **2017**, *19*, 4092−4117.

(18) Fang, R.; Dhakshinamoorthy, A.; Li, Y.; Garcia, H. Metal Organic Frameworks for Biomass Conversion. *Chem. Soc. Rev.* **2020**, *49*, 3638−3687.

(19) Franco, A.; Negi, A.; Luque, R.; Carrillo-Carrión, C. Selectivity Control in the Oxidative Ring-Opening of Dimethylfuran Mediated by Zeolitic-Imidazolate Framework-8 Nanoparticles. *ACS Sustainable Chem. Eng.* **2021**, *9*, 8090−8096.

(20) Park, K. S.; Ni, Z.; Côté, A. P.; Choi, J. Y.; Huang, R.; Uribe-Romo, F. J.; Chae, H. K.; O'Keeffe, M.; Yaghi, O. M. Exceptional Chemical and Thermal Stability of Zeolitic Imidazolate Frameworks. *Proc. Natl. Acad. Sci. U.S.A.* **2006**, *103*, 10186−10191.

(21) Zheng, Z.; Rong, Z.; Nguyen, H. L.; Yaghi, O. M. Structural Chemistry of Zeolitic Imidazolate Frameworks. *Inorg. Chem.* **2023**, *62*, 20861−20873.

(22) Phan, A.; Doonan, C. J.; Uribe-Romo, F. J.; Knobler, C. B.; O'Keeffe, M.; Yaghi, O. M. Synthesis, Structure, and Carbon Dioxide Capture Properties of Zeolitic Imidazolate Frameworks. *Acc. Chem. Res.* **2010**, *43*, 58−67.

(23) Wang, H.; Pei, X.; Kalmutzki, M. J.; Yang, J.; Yaghi, O. M. Large Cages of Zeolitic Imidazolate Frameworks. *Acc. Chem. Res.* **2022**, *55*, 707−721.

(24) Odoh, S. O.; Cramer, C. J.; Truhlar, D. G.; Gagliardi, L. Quantum-Chemical Characterization of the Properties and Reactivities of Metal-Organic Frameworks. *Chem. Rev.* **2015**, *115*, 6051−6111.

(25) Chizallet, C.; Lazare, S.; Bazer-Bachi, D.; Bonnier, F.; Lecocq, V.; Soyer, E.; Quoineaud, A. A.; Bats, N. Catalysis of Transesterification by a Nonfunctionalized Metal-Organic Framework: Acido-Basicity at the External Surface of ZIF-8 Probed by FTIR and ab Initio Calculations. *J. Am. Chem. Soc.* **2010**, *132*, 12365−12377.

(26) Spicher, S.; Grimme, S. Robust Atomistic Modeling of Materials, Organometallic, and Biochemical Systems. *Angew. Chem., Int. Ed.* **2020**, *59*, 15665−15673.

(27) Bannwarth, C.; Caldeweyher, E.; Ehlert, S.; Hansen, A.; Pracht, P.; Seibert, J.; Spicher, S.; Grimme, S. Extended Tight-Binding Quantum Chemistry Methods. *WIREs Comput. Mol. Sci.* **2021**, *11*, No. e1493.

(28) Pracht, P.; Bohle, F.; Grimme, S. Automated Exploration of the Low-Energy Chemical Space with Fast Quantum Chemical Methods. *Phys. Chem. Chem. Phys.* **2020**, *22*, 7169−7192.

(29) Spicher, S.; Bursch, M.; Grimme, S. Efficient Calculation of Small Molecule Binding in Metal−Organic Frameworks and Porous Organic Cages. *J. Phys. Chem. C* **2020**, *124* (50), 27529−27541.

(30) Perdew, J. P.; Burke, K.; Ernzerhof, M. Generalized Gradient Approximation Made Simple. *Phys. Rev. Lett.* **1996**, *77*, No. 3865.

(31) Kresse, G.; Furthmüller, J. Efficient Iterative Schemes for Ab Initio Total-Energy Calculations Using a Plane-Wave Basis Set. *Phys. Rev. B* **1996**, *54*, No. 11169.

(32) Kresse, G.; Furthmüller, J. Efficiency of Ab-Initio Total Energy Calculations for Metals and Semiconductors Using a Plane-Wave Basis Set. *Comput. Mater. Sci.* **1996**, *6*, 15−50.

(33) Grimme, S.; Antony, J.; Ehrlich, S.; Krieg, H. A Consistent and Accurate Ab Initio Parametrization of Density Functional Dispersion Correction (DFT-D) for the 94 Elements H-Pu. *J. Chem. Phys.* **2010**, *132*, No. 154104.

(34) Grimme, S.; Ehrlich, S.; Goerigk, L. Effect of the Damping Function in Dispersion Corrected Density Functional Theory. *J. Comput. Chem.* **2011**, *32*, 1456−1465.

(35) Kresse, G.; Joubert, D. From Ultrasoft Pseudopotentials to the Projector Augmented-Wave Method. *Phys. Rev. B* **1999**, *59*, No. 1758.

(36) Monkhorst, H. J.; Pack, J. D. Special Points for Brillouin-zone Integrations. *Phys. Rev. B* **1976**, *13*, No. 5188.

(37) Henkelman, G.; Jónsson, H. Improved Tangent Estimate in the Nudged Elastic Band Method for Finding Minimum Energy Paths and Saddle Points. *J. Chem. Phys.* **2000**, *113*, 9978−9985.

(38) Heyden, A.; Bell, A. T.; Keil, F. J. Efficient Methods for Finding Transition States in Chemical Reactions: Comparison of Improved Dimer Method and Partitioned Rational Function Optimization Method. *J. Chem. Phys.* **2005**, *123*, No. 224101.

(39) Cusinato, L.; del Rosal, I.; Poteau, R. Shape, Electronic Structure and Steric Effects of Organometallic Nanocatalysts: Relevant Tools to Improve the Synergy between Theory and Experiment. *Dalton Trans.* **2017**, *46*, 378−395.

(40) Frisch, M. J.; Trucks, G. W.; Schlegel, H. B.; Scuseria, G. E.; Robb, M. A.; Cheeseman, J. R.; Scalmani, G.; Barone, V.; Petersson, G. A.; Nakatsuji, H.; Li, X.; Caricato, M.; Marenich, A. V.; Bloino, J.; Janesko, B. G.; Gomperts, R.; Mennucci, B.; Hratchian, H. P.; Ortiz, J. V.; Izmaylov, A. F.; Sonnenberg, J. L.; Williams-Young, D.; Ding, F.; Lipparini, F.; Egidi, F.; Goings, J.; Peng, B.; Petrone, A.; Henderson, T.; Ranasinghe, D.; Zakrzewski, V. G.; Gao, J.; Rega, N.; Zheng, G.; Liang, W.; Hada, M.; Ehara, M.; Toyota, K.; Fukuda, R.; Hasegawa, J.; Ishida, M.; Nakajima, T.; Honda, Y.; Kitao, O.; Nakai, H.; Vreven, T.; Throssell, K.; Montgomery, J. A., Jr.; Peralta, J. E.; Ogliaro, F.; Bearpark, M. J.; Heyd, J. J.; Brothers, E. N.; Kudin, K. N.; Staroverov, V. N.; Keith, T. A.; Kobayashi, R.; Normand, J.; Raghavachari, K.; Rendell, A. P.; Burant, J. C.; Iyengar, S. S.; Tomasi, J.; Cossi, M.; Millam, J. M.; Klene, M.; Adamo, C.; Cammi, R.; Ochterski, J. W.; Martin, R. L.; Morokuma, K.; Farkas, O.; Foresman, J. B.; Fox, D. J. *Gaussian 16, Revision C.01*; Gaussian, Inc.: Wallingford CT, 2016.

(41) Weigend, F.; Ahlrichs, R. Balanced Basis Sets of Split Valence, Triple Zeta Valence and Quadruple Zeta Valence Quality for H to Rn: Design and Assessment of Accuracy. *Phys. Chem. Chem. Phys.* **2005**, *7*, 3297−3305.

(42) Becke, A. D. Density-Functional Exchange-Energy Approximation with Correct Asymptotic Behavior. *Phys. Rev. A* **1988**, *38*, No. 3098.

(43) Lee, C.; Yang, W.; Parr, R. G. Development of the Colle-Salvetti Correlation-Energy Formula into a Functional of the Electron Density. *Phys. Rev. B* **1988**, *37*, No. 785.

(44) Tao, J. M.; Perdew, J. P.; Staroverov, V. N.; Scuseria, G. E. Climbing the Density Functional Ladder: Nonempirical Meta-Generalized Gradient Approximation Designed for Molecules and Solids. *Phys. Rev. Lett.* **2003**, *91*, No. 146401.

(45) Zhao, Y.; Truhlar, D. G. A New Local Density Functional for Main-Group Thermochemistry, Transition Metal Bonding, Thermochemical Kinetics, and Noncovalent Interactions. *J. Chem. Phys.* **2006**, *125*, No. 194101.

(46) Adamo, C.; Barone, V. Toward Reliable Density Functional Methods without Adjustable Parameters: The PBE0 Model. *J. Chem. Phys.* **1999**, *110*, 6158−6169.

(47) Becke, A. D. Density-Functional Thermochemistry. III. The Role of Exact Exchange. *J. Chem. Phys.* **1993**, *98*, 5648−5652.

(48) Staroverov, V. N.; Scuseria, G. E.; Tao, J.; Perdew, J. P. Comparative Assessment of a New Nonempirical Density Functional: Molecules and Hydrogen-Bonded Complexes. *J. Chem. Phys.* **2003**, *119*, 12129−12137.

(49) Zhao, Y.; Truhlar, D. G. The M06 Suite of Density Functionals for Main Group Thermochemistry, Thermochemical Kinetics, Noncovalent Interactions, Excited States, and Transition Elements: Two New Functionals and Systematic Testing of Four M06-Class Functionals and 12 Other Functionals. *Theor. Chem. Acc.* **2008**, *120*, 215−241.

(50) Neese, F. Software update: The ORCA program system—Version 5.0. *WIREs Comput. Mol. Sci.* **2022**, *12*, No. e1606.

(51) Hellweg, A.; Hättig, C.; Höfener, S.; Klopper, W. Optimized Accurate Auxiliary Basis Sets for RI-MP2 and RI-CC2 Calculations for the Atoms Rb to Rn. *Theor. Chem. Acc.* **2007**, *117*, 587−597.

(52) Guo, Y.; Riplinger, C.; Becker, U.; Liakos, D. G.; Minenkov, Y.; Cavallo, L.; Neese, F. Communication: An Improved Linear Scaling Perturbative Triples Correction for the Domain Based Local Pair-Natural Orbital Based Singles and Doubles Coupled Cluster Method [DLPNO-CCSD(T)]. *J. Chem. Phys.* **2018**, *148*, No. 011101.

(53) Bo, C.; Maseras, F.; López, N. The Role of Computational Results Databases in Accelerating the Discovery of Catalysts. *Nat. Catal.* **2018**, *1*, 809−810.

(54) Álvarez-Moreno, M.; De Graaf, C.; López, N.; Maseras, F.; Poblet, J. M.; Bo, C. Managing the Computational Chemistry Big Data Problem: the ioChem-BD Platform. *J. Chem. Inf. Model.* **2015**, *55*, 95−103.

(55) ZIFs *ioChem-BD Computational Chemistry Database*, https://iochem-bd.bsc.es/browse/handle/100/438876 DOI: 10.19061/iochem-bd-6-521.

(56) Jablonka, K. M.; Rosen, A. S.; Krishnapriyan, A. S.; Smit, B. An Ecosystem for Digital Reticular Chemistry. *ACS Cent. Sci.* **2023**, *9*, 563−581.

(57) Description of Featurizers Implemented in MOFDSCRIBE. https://mofdscribe.readthedocs.io/en/latest/api/featurizers. (accessed 12/01/25).

(58) Jablonka, K. M.; Ongari, D.; Moosavi, S. M.; Smit, B. Big-Data Science in Porous Materials: Materials Genomics and Machine Learning. *Chem. Rev.* **2020**, *120*, 8066−8129.

(59) Fairen-Jimenez, D.; Moggach, S. A.; Wharmby, M. T.; Wright, P. A.; Parsons, S.; Düren, T. Opening the Gate: Framework Flexibility in ZIF-8 Explored by Experiments and Simulations. *J. Am. Chem. Soc.* **2011**, *133*, 8900−8902.

(60) Todeschini, R.; Consonni, V. *Handbook of Chemoinformatics*; Wiley-VCH Verlag GmbH:: Weinheim, Germany, 2008; pp 1004−1033.

(61) Arteca, G. A. *Reviews in Computational Chemistry*; John Wiley & Sons, Inc.: Hoboken, NJ, USA, 2007; pp 191−253.

(62) Wirth, M.; Volkamer, A.; Zoete, V.; Rippmann, F.; Michielin, O.; Rarey, M.; Sauer, W. H. B. Protein Pocket and Ligand Shape Comparison and Its Application in Virtual Screening. *J. Comput.-Aided Mol. Des.* **2013**, *27*, 511−524.

(63) Zhang, R. Z.; Seth, S.; Cumby, J. Grouped Representation of Interatomic Distances as a Similarity Measure for Crystal Structures. *Digital Discovery* **2023**, *2*, 81−90.

(64) Ongari, D.; Boyd, P. G.; Barthel, S.; Witman, M.; Haranczyk, M.; Smit, B. Accurate Characterization of the Pore Volume in Microporous Crystalline Materials. *Langmuir* **2017**, *33*, 14529−14538.

(65) Willems, T. F.; Rycroft, C. H.; Kazi, M.; Meza, J. C.; Haranczyk, M. Algorithms and Tools for High-Throughput Geometry-Based Analysis of Crystalline Porous Materials. *Micropor. Mesopor. Mater.* **2012**, *149*, 134−141.

(66) Waskom, M. L. Seaborn: Statistical Data Visualization. *J. Open Source Software* **2021**, *6* (60), No. 3021.

(67) Sever, R. R.; Root, T. W. Computational Study of Tin-Catalyzed Baeyer−Villiger Reaction Pathways Using Hydrogen Peroxide as Oxidant. *J. Phys. Chem. B* **2003**, *107*, 10848−10862.

(68) Yamabe, S.; Yamazaki, S. The Role of Hydrogen Bonds in Baeyer−Villiger Reactions. *J. Org. Chem.* **2007**, *72*, 3031−3041.

(69) Intermediates **6a** are obtained by following the eigenvector of the lowest-energy TS **TS6a**.

(70) Ernst, M.; Evans, J. D.; Gryn'ova, G. Host−Guest Interactions in Framework Materials: Insight from Modeling. *Chem. Phys. Rev.* **2023**, *4*, No. 041303.

(71) Moghadam, P. Z.; Fairen-Jimenez, D.; Snurr, R. Q. Efficient Identification of Hydrophobic MOFs: Application in the Capture of Toxic Industrial Chemicals. *J. Mater. Chem. A* **2016**, *4*, 529−536.

(72) Mouarrawis, V.; Plessius, R.; van der Vlugt, J. I.; Reek, J. N. H. Confinement Effects in Catalysis Using Well-Defined Materials and Cages. *Front. Chem.* **2018**, *6*, No. 623.

(73) Hobday, C. L.; Bennett, T. D.; Fairen-Jimenez, D.; Graham, A. J.; Morrison, C. A.; Allan, D. R.; Düren, T.; Moggach, S. A. Tuning the Swing Effect by Chemical Functionalization of Zeolitic Imidazolate Frameworks. *J. Am. Chem. Soc.* **2018**, *140*, 382−387.

(74) Titi, H. M.; Marrett, J. M.; Dayaker, G.; Arhangelskis, M.; Mottillo, C.; Morris, A. J.; Rachiero, G. P.; Friščić, T.; Rogers, R. D. Hypergolic Zeolitic Imidazolate Frameworks (ZIFs) as next-Generation Solid Fuels: Unlocking the Latent Energetic Behavior of ZIFs. *Sci. Adv.* **2019**, *5*, No. eaav9044.

(75) Sun, Q.; He, H.; Gao, W.-Y.; Aguila, B.; Wojtas, L.; Dai, Z.; Li, J.; Chen, Y.-S.; Xiao, F.-S.; Ma, S. Imparting Amphiphobicity on Single-Crystalline Porous Materials. *Nat. Commun.* **2016**, *7*, No. 13300.

(76) Li, K.; Olson, D. H.; Seidel, J.; Emge, T. J.; Gong, H.; Zeng, H.; Li, J. Zeolitic Imidazolate Frameworks for Kinetic Separation of Propane and Propene. *J. Am. Chem. Soc.* **2009**, *131*, 10368−10369.

(77) Chaplais, G.; Fraux, G.; Paillaud, J.-L.; Marichal, C.; Nouali, H.; Fuchs, A. H.; Coudert, F.-X.; Patarin, J. Impacts of the Imidazolate Linker Substitution (CH_3, Cl, or Br) on the Structural and Adsorptive Properties of ZIF-8. *J. Phys. Chem. C* **2018**, *122*, 26945−26955.

(78) Karagiaridi, O.; Lalonde, M. B.; Bury, W.; Sarjeant, A. A.; Farha, O. K.; Hupp, J. T. Opening ZIF-8: A Catalytically Active Zeolitic Imidazolate Framework of Sodalite Topology with Unsubstituted Linkers. *J. Am. Chem. Soc.* **2012**, *134*, 18790−18796.

(79) Morris, W.; Doonan, C. J.; Furukawa, H.; Banerjee, R.; Yaghi, O. M. Crystals as Molecules: Postsynthesis Covalent Functionalization of Zeolitic Imidazolate Frameworks. *J. Am. Chem. Soc.* **2008**, *130*, 12626−12627.

(80) For instance for ZIF-Vinyl, the Gibbs energy barrier with the re-optimized cell was 1.21 eV, which is less than 0.1 eV from the value with the non-optimized cell (1.27 eV).

(81) Willems, T. F.; Rycroft, C. H.; Kazi, M.; Meza, J. C.; Haranczyk, M. Algorithms and Tools for High-Throughput Geometry-based Analysis of Crystalline Porous Materials. *Micropor. Mesopor. Mater.* **2012**, *149*, 134−141.